

Modelling CO emission from Mira's wind

N. Ryde

Uppsala Astronomical Observatory, Box 515, SE-751 20, Uppsala, Sweden

ryde@astro.uu.se

and

F.L. Schöier

Stockholm Observatory, SE-133 36 Saltsjöbaden, Sweden

fredrik@astro.su.se

ABSTRACT

We have modelled the circumstellar envelope of *o* Ceti (Mira) using new observational constraints. These are obtained from photospheric light scattered in near-IR vibrational-rotational lines of circumstellar CO molecules at $4.6\ \mu\text{m}$: absolute fluxes, the radial dependence of the scattered intensity, and two line ratios. Further observational constraints are provided by ISO observations of far-IR emission lines from highly excited rotational states of the ground vibrational state of CO, and radio observations of lines from rotational levels of low excitation of CO. A code based on the Monte-Carlo technique is used to model the circumstellar line emission.

The vibrational-rotational lines are sensitive to the radiation field, whereas the pure rotational lines, such as the rotational lines of low excitation measured at radio wavelengths and the rotational lines from highly excited states observed with ISO, are usually more sensitive to the temperature structure. These rotational lines have been the prime probe in most earlier investigations.

We find that it is possible to model the radio and ISO fluxes, as well as the highly asymmetric radio-line profiles, reasonably well with a spherically symmetric and smooth stellar wind model. However, it is not possible to reproduce the observed NIR line fluxes consistently with a 'standard model' of the stellar wind. This is probably due to incorrectly specified conditions of the inner regions of the wind model, since the stellar flux needs to be larger than what is obtained from the standard model at the point of scattering, i.e., the intermediate regions at approximately $100\text{--}400 R_*$ ($2''\text{--}7''$) away from the star. Thus, the optical depth in the vibrational-rotational lines from the star to the point of scattering has to be decreased. This can be accomplished in several ways. For instance, the gas close to the star (within approximately $2''$) could be in such a form that light is able to pass through, either due to the medium being clumpy or by the matter being in radial structures (which, further out, develops into more smooth or shell-like structures). Further observations of the gas in the stellar wind close to Mira are required to resolve this problem.

The model circumstellar envelope, which reproduces the observables reasonably well, has a mass-loss rate of $2.5 \times 10^{-7} M_{\odot} \text{yr}^{-1}$, and a turbulent velocity of 1.5 km s^{-1} , given a terminal expansion velocity of the wind of 2.5 km s^{-1} .

Subject headings: stars: AGB and post-AGB — circumstellar matter — late-type — mass-loss — infrared: stars

1. INTRODUCTION

The inner regions of circumstellar envelopes around asymptotic giant branch stars are still enigmatic. These regions, located further out than the pulsating outer atmosphere but typically within 100 stellar radii, are of interest for several reasons; The circumstellar wind is accelerated here to its terminal velocity, the chemistry is ‘frozen out’ approximately at its photospheric values, and dust nucleation and growth take place. This is important for the mass loss of the star, a process we do not understand how and why it occurs. For example, we do not know whether matter is ejected in puffs or in a steady, homogeneous wind. The mass loss returns matter to the interstellar medium and plays a vital role in the cosmic cycling and enrichment of matter, see for example Gustafsson and Ryde (2000). In order to study these inner regions we need to observe them in detail. However, very few observational constraints exist on the conditions in these complex regions.

By combining observations, sampling gas located at a distance on the sky of approximately $1''$ and beyond, and a detailed modelling of the circumstellar envelopes one might be able to put constraints on the inner regions. Ryde et al. (2000) observed scattered photospheric light in circumstellar vibration-rotational lines of CO $2''-7''$ away from Mira. They analysed the emission lines from the circumstellar envelope using a simple analytic approach, an analysis which suggested a time constant mass-loss rate, when averaged over 100 years, over the past 1200 years. In this paper we present a detailed analysis both of these observations and of those which tell us about the properties of the whole envelope. The modelling presented here provides a better insight into the conditions close to the star, and gives a larger degree of flexibility to test different models.

o Ceti (Mira or HD 14386) is the prototype of the mira class of long-period variables with characteristic pseudo-periodic brightness variations in time. They are cool, red giants on the asymptotic giant branch (AGB) with considerable mass-loss rates and circumstellar envelopes (CSEs) of large extension. The visual-light variations are related to large-amplitude radial pulsations which cause a large variation of the effective temperature. Note, that *o* Ceti is a binary system. The angular dis-

tance between Mira A and the hot, compact companion star Mira B (VZ Ceti) is $0.6''$ (Karovska et al. 1993; 1997). The companion could be a white dwarf with a mass of about $1 M_{\odot}$, a luminosity of $2 L_{\odot}$, and a temperature of more than 30000 K [these parameters are based on an analysis of International Ultraviolet Explorer (IUE) spectra by Stickland et al. (1982)]. Danchi et al. (1994) suggest it is embedded in an accretion disk, giving rise to an abnormal illumination of Mira A.

In general, the kinematics, the density and the temperature structures of CSEs of AGB stars seem to be relatively simple, with an over-all spherical symmetry prevailing (see, e.g., Olofsson 1996). The stable and abundant CO molecule is self-shielding (Glassgold 1996) and therefore of approximately constant abundance through out the envelope. However, the chemical structure is certainly quite complex, restricting us to schematic modelling of these objects [see for example Glassgold (1996)]. The lack of spatial resolution in the observations, nonetheless suggesting more complex geometries (e.g., Stanek et al. 1995), also hampers the analysis.

The observations of CO lines at millimeter wavelength in Mira’s wind indicate some complexity. An asymmetry is clearly visible in the radio-line profiles. A number of suggestions in the literature have been made for multi-wind scenarios, such as winds of different characteristics, jets, or other phenomena which introduce dramatic variations in the envelope structure with distance. Thus, several combinations exist of mass-loss rates, expansion and turbulent velocities, which are able to reproduce the radio-line profiles fairly well. This means, for instance, that there is no consensus as regards the actual expansion velocity of Mira’s wind. Crosas et al. (1997) experiment with an expansion velocity (v_e) of approximately 2 km s^{-1} and a turbulent velocity (v_t) of approximately 4 km s^{-1} in their version of the inner wind, while Young (1995) arrived at $v_e=4.8 \text{ km s}^{-1}$. However, Young (1995) points out that the wings show an expansion velocity of 10 km s^{-1} . Knapp et al. (1998) model a fast outer wind with a mass-loss rate of $\dot{M}=4.4 \times 10^{-7} M_{\odot} \text{ yr}^{-1}$, and an expansion velocity of $6.7 \pm 1.0 \text{ km s}^{-1}$. An inner wind is supposed to be a resumed wind in analogy with the detached shells found in four carbon stars (Olofsson

et al. 1996). This slow wind component has a lower mass-loss rate and a much lower expansion velocity than what is found normally in Miras; $\dot{M}=9.4\times 10^{-8} M_{\odot} \text{ yr}^{-1}$ and $v_e=2.4\pm 0.4 \text{ km s}^{-1}$. Planesas et al. (1990a) interpret the CO $J=1\rightarrow 0$ and $J=2\rightarrow 1$ lines as partly originating from a spherically symmetric CSE with $v_e=3 \text{ km s}^{-1}$.

Numerous high-resolution, optical and infrared wavelength measurements provide evidence that Mira itself is elongated (e.g., Karovska et al. 1991, 1997; Haniff et al. 1992; Wilson et al. 1992; Quirrenbach et al. 1992). Karovska et al. (1997) suggest that the asymmetry could be due to unresolved bright spots or non-radial pulsation, or even a wind interaction with Mira B. As an alternative to an asymmetric atmosphere, Danchi et al. (1994) discussed the possibility of the observed asymmetries being caused by non-uniform dust shells close to the star. Also Planesas et al. (1990a,b) interpreted their asymmetric CO $J=1\rightarrow 0$ and $J=2\rightarrow 1$ line profiles and brightness maps, which are at a spatial resolution of $6''$, as originating partly from a very slow, partially collimated wind, due to high densities of gas in the equatorial plane close to the star.

We will, nevertheless, assume a spherically symmetric model for the CSE since the situation is unclear as regards the physical origin of the complexity, and its dependence on the distance from the star. Also, Ryde et al. (2000) concluded from their near-IR (NIR) CO line data that they do not necessarily indicate a non-symmetric, inner wind.

2. OBSERVATIONAL DATA

Our modelling of Mira's wind will be compared with three sets of observations probing different regions of the CSE.

First, spatially and spectrally resolved, vibrational-rotational line emission from the CO fundamental band lying at $4.6 \mu\text{m}$ is used as a probe of the inner regions (Ryde et al. 2000). The lines observed are R(1), R(2), and R(3). These emission lines consist of photospheric light scattered by CO molecules in the intermediate regions (approximately $100\text{--}400 R_{*}$) of the CSE around Mira. These observations are the most important ones in the discussion presented here, providing a new constraint to the modelling of the CSE. The emission lines were detected in observations with the

Phoenix spectrometer mounted on the 4 m Mayall telescope at Kitt Peak. The reduction and absolute flux calibration of these observations are described by Ryde et al. (2000). The uncertainties in the absolute fluxes are probably lower than $\pm 50\%$, which we regard as a conservative estimate.

Second, as a further constraint on our model we have retrieved far-IR (FIR) observations of Mira, which probe regions within $2''$ ($\lesssim 100 R_{*}$) of the star, obtained with the Infrared Space Observatory (ISO) (Kessler et al. 1996). These high-lying rotational lines of ^{12}CO are retrieved from the ISO-data archive¹. The Long Wavelength Spectrometer (LWS, Clegg et al. 1996) was used in the grating mode (LWS01) providing a mean spectral resolution element of approximately $0.7 \mu\text{m}$. We will discuss only the line-integrated fluxes. The 32 minutes of observations were performed in the morning the 4th July 1997 during ISO revolution 596. The reductions were made using the most recent pipeline, basic reduction package OLP (v.7) and the ISO Spectral Analysis Package (ISAP v.1.5). The pipeline processing of the data, such as the flux calibration, is described by Swinyard et al. (1996); the combined absolute and systematic uncertainties in the fluxes are large, of the order $\pm 50\%$. Mira is considered to be a faint source in the ISO-LWS reduction procedures (Flux $< 50 \text{ Jy}$ at $120 \mu\text{m}$). The observations consist of weak emission lines on a strong continuum. A large uncertainty is introduced in the subtraction of the continuum. We have measured the emission intensities in the same manner as is described in Ryde et al. (1999c) for IRAS 15194-5115. The lines studied are $J=19\rightarrow 18$, $J=18\rightarrow 17$, $J=17\rightarrow 16$, $J=16\rightarrow 15$, at 137.2, 144.7, 153.3, and $162.9 \mu\text{m}$, respectively. The line-integrated fluxes measured yield a mean flux of approximately $(2 \pm 1) \times 10^{-20} \text{ W cm}^{-2}$ for the four lines.

Third, radio observations, made with the James Clerk Maxwell Telescope (JCMT) on Hawaii, of the CO $J=2\rightarrow 1$, $J=3\rightarrow 2$, and $J=4\rightarrow 3$ lines are retrieved from the public archive of the JCMT². These data are taken at face value. By compar-

¹This project is partly based on observations with ISO, an ESA project with instruments funded by ESA Member States (especially the PI countries: France, Germany, the Netherlands and the United Kingdom) and with the participation of ISAS and NASA. <http://isowww.estec.esa.nl/>
²<http://www.jach.hawaii.edu/>

ing different observations we estimate the uncertainty in the intensity scale to be approximately $\pm 20\%$. The intensity scale is given in main-beam brightness temperature, T_{mb} . These data provide constraints on the outer regions of the CSE, i.e., approximately $1000 R_*$ away from the star and beyond.

In Tables 2, and 3 the observational results of the NIR, ISO, and JCMT observations are presented. In Table 2, the mean values of the NIR line intensities obtained west, east, north, and south (Ryde et al. 2000) are given, as well as the R(1)/R(3) and R(2)/R(3)-line ratios. The intensities are means for a position $(2 \pm 0.5)''$ away from the star, the ratios are means over the distance $2-3.4''$. Table 2 also presents the radial brightness distribution of the NIR line emission given as the exponent of the intensity power-law ($\text{dlog } I/\text{dlog } \beta$) of the R(2) vibrational-rotational line and is a mean over the entire range (β is the angular distance from the star on the sky). The uncertainties quoted for the line ratios and the slope are pure measurement uncertainties. The R(1)/R(3) ratio in Table 2 may be uncertain due to systematic uncertainties in R(1), cf. Ryde et al. (2000). The ISO flux in Table 3 is given as the mean of the four measured lines in order to reduce the uncertainty since the data is noisy and the line intensities should not vary much.

3. THE MODEL OF THE CIRCUMSTELLAR ENVELOPE

We have used a Monte-Carlo (MC) approach to the multi-level, non-LTE, radiative-transfer problem when modelling the circumstellar wind of Mira. We have applied the methodology of Bernes (1979) to the transfer of line-radiation of CO in a spherically symmetric and smooth CSE, formed by a constant mass-loss rate, and expanding at a constant velocity. The inner and outer radii of the CSE are used as the input for the modelling. For a more detailed description of the modelling, see Schöier (2000).

The model is constructed by iteratively solving the equations of radiative transfer and the statistical equilibrium equations for the level populations of ^{12}CO . The solution is found when a steady state of the populations, as a function of radial distance from the star, is achieved. The source

function of the entire wind is thereby known, which makes possible a straight-forward calculation of the spectrum by the solution of the radiative transfer through the envelope along the line-of-sight, resulting in predicted intensities of the observed spectral lines as a function of the distance from the star.

A draw-back of Monte-Carlo simulations in general is the slow convergence, typically scaling with $\sqrt{N_{\text{iter}}}$. On the other hand, the advantages are several. The programming can be done in close relation to the physical reality; the radiation field can be taken into account in a correct manner, and inhomogeneities and complex geometries are relatively easily implemented. Velocity fields and gradients of any size are allowed in the programming.

In our MC model, complete angular and frequency redistribution is assumed, the absorption and the emission profiles being the same. Thus, the local emission is assumed to be isotropic and the scattering is assumed to be incoherent. The distribution of frequency shifts given by the emission profile is defined by a gaussian Doppler profile:

$$\Phi(\nu) = \frac{1}{\sigma\sqrt{\pi}} \exp \left[\frac{-(\nu - \nu_0 - \vec{v} \cdot \vec{n} \nu_0/c)^2}{\sigma^2} \right]. \quad (1)$$

The width of this profile, σ , is given by the local, thermal broadening and the micro-turbulent broadening. The velocity field in the expanding wind will allow shifts from the line centre as given in the laboratory frame, ν_0 . The velocity field is represented by the vector \vec{v} and the direction of the beam, i.e. the random direction of one emitted photon, by the unit vector \vec{n} .

For the rotational transitions, with spontaneous de-excitation rates of the order of 10^{-7} s^{-1} , the assumption of complete frequency redistribution (CRD) is a good assumption, since the collisions will have time to reset the frequency-memory of the excited atoms. However, for the vibrational-rotational transitions, with rates of the order of 10 s^{-1} , this assumption may be a fallacy. For these infrared transitions, photons are more likely coherently scattered in frequency. The more scattering events, i.e., the higher the radial optical depth in the wind, the more important it is that the model is made to properly take into account coherent

scattering in the model.

By dividing every NIR transition into a large number of subdivisions, but conserving the overall line profile, we are able to simulate coherent scattering in the MC code. The absorption and the emission profiles are assumed to be the same. We find that for optical depths of the order of 50 or less, the difference between a CRD and a coherent description of the NIR transitions is less than the numerical noise, which is intrinsic to the MC method. For a Mira model with a CSE with an inner radius at $13 R_*$, the radial optical depth is approximately 40, which motivates our approach to run the model with all transitions in CRD.

4. MODEL PARAMETERS

Measurements of the multi-wavelength angular diameter of Mira (Haniff et al. 1995), combined with trigonometric parallaxes measured with the Hipparcos satellite (Van Leeuwen et al. 1997), suggest a mean radius of $(464 \pm 80) R_\odot$. The distance to Mira is (128_{-15}^{+20}) pc (ESA 1997). From Mahler et al. (1997) one can derive a bolometric luminosity $L_{\text{tot}}=8900 L_\odot$, a temperature $T_{\text{eff}}=2400$ K and a radius of $550 R_\odot=3.8 \times 10^{13}$ cm for the phase of *o* Ceti at October 29, 1998, the date the NIR observations were made, see Figure 1. Mira was at its maximum radius at this epoch according to Mahler et al. (1997). The ISO and radio data were observed at other times, but are not as sensitive to the radiation field, and thereby to the phases of Mira, as the NIR data. These values of the model parameters of Mira are consistent with the corresponding values obtained by, among others, Danchi et al. (1994) and Haniff et al. (1995). These authors arrive at similar temperatures; a mean (over phases) effective temperature of $T_{\text{eff}} \sim 2800$ K. The terminal expansion velocity is set to be $v_e=2.5 \text{ km s}^{-1}$ (Knapp et al. 1998). The model parameters we have adopted are given in Table 1.

The radiative energy input to the wind system originates from the central star and is specified by a luminosity and an effective temperature of the star and by a luminosity and effective temperature of the surrounding dust, cf. Table 1. Since the dust is concentrated close to the star (Bester et al. 1991), the ambient radiation from the dust further out in the CSE is considered to

be small and it is not taken into account in our model. The dust will absorb part of the stellar flux and re-radiate it in the infrared as thermal radiation. Lopez et al. (1997) fit their observations with two spherically symmetric dust shells at 3 and 10 stellar radii, with inhomogeneities or clumps embedded in the spherically symmetric dust shells. Danchi et al. (1994) fit their observations with a dust distribution which peaks at 2.7 stellar radii away from the star, and where the temperature is 1050–1300 K, depending on phase. Also Bester et al. (1991) deduced an inner extension of the dust shell of about three stellar radii, and a dust temperature of 1200 K. Thus, the spatial dust distribution peaks at approximately 3 stellar radii with a temperature of about 1100 K, leading to an upper limit of the re-radiated luminosity of 30% of the total bolometric luminosity; $2700 L_\odot$. Haniff et al. (1995) found, however, that the circumstellar dust in Mira contributes less than 20% of the bolometric luminosity. We therefore set the dust luminosity to be $1800 L_\odot$, implying a stellar contribution of $7100 L_\odot$. The former radiation, which is mainly in the infrared, is important for pumping vibrational states, leading to non-thermal level populations of the rotational states which could affect the NIR line intensities. Hence, we model the inner energy source with a spectral energy distribution consisting of two black-bodies, using the temperatures and luminosities above, see also Table 1.

The kinetic temperature structure of the gas affects the CO level populations through collisions, modelled through collisional rates [see the discussion by Ryde et al. (1999c)] which are functions of the temperature. The temperature also affects the thermal broadening of the absorption and emission profiles. These are, however, mostly determined by the larger turbulent velocity. The gas temperature structure of the CSE can be calculated in a self-consistent way in our model, by solving the energy balance equation of the system (cf. Ryde et al. 1999c). However, in the present discussion we select, for simplicity, a structure of the gas kinetic temperature in the wind according to:

$$T(r) = T_0 \left(\frac{10^{15} \text{ cm}}{r} \right)^\zeta, \quad (2)$$

where the exponent $\zeta \approx 1$, see for example Kahane and Jura (1994). T_0 is the temperature at 10^{15} cm

and r is the distance from the star in centimeters. This kinetic temperature structure and the excitation temperature structures calculated by the model are shown in Figure 3b.

Mira B certainly also adds mechanical energy to the circumstellar environment, which will lead to an additional heating. The NIR lines are, however, radiatively excited and not greatly affected by the kinetic temperature of the surrounding gas/dust. The radio lines may, however, in principle be affected by their kinetic environment, but are formed further out where the influence of the binary star can be considered to be small.

The CSE is characterised by the mass-loss rate of the star and the expansion velocity of the wind, which together give the density as a function of the radial distance from the star. The density of CO will depend on the fractional abundance of CO relative to the abundance of hydrogen molecules, H_2 . This fractional abundance of ^{12}CO molecules is assumed to be $f_{CO}=5\times 10^{-4}$ (Knapp et al. 1998) throughout the wind. This is a value generally used for oxygen-rich envelopes, and the same value was adopted in Ryde et al. (2000). In the case of Mira the mass-loss rate is relatively small, leading to an increased importance of the radiation field, especially for the NIR lines; see the discussion on the dusty envelope of the object IRAS 15194-5115 with a high mass-loss rate, where the vibrational-rotational transitions are found to be unimportant (Ryde et al. 1999c).

The ^{12}CO molecule data are the same as those used by Ryde et al. (1999c). We use 30 rotational levels for each of the ground and first vibrational states. This is generally sufficient in order to treat the CO excitation in CSEs properly, cf. Ryde et al. (1999c). The collisional rates of the NIR vibrational-rotational transitions are much smaller than the radiative de-excitation rates and they are set at zero in the model (see for example Ryde et al. 1999a). The collisional rates of pure rotational transitions are non-zero. Kirby-Docken and Liu (1978) provide oscillator strengths, which for our transitions are consistent with Huré and Roueff (1996)³.

The photo-dissociation radius of the CO envelope (r_p) is determined by the interstellar UV-field (Mamon et al. 1988). In the case of Mira, this

value is relatively uncertain. We apply an outer radius of the CO shell of 2×10^{16} cm, which corresponds to a diameter of about $20''$ at the distance of Mira of 128 pc, cf. Planesas et al. (1990b).

5. RESULTS PRODUCED BY THE MODEL

For objects with low mass-loss rates, the NIR, vibrational-rotational lines are sensitive to the stellar intensity, whereas pure rotational lines, such as the low rotational lines measured at radio wavelengths and the higher rotational lines observed with ISO are usually more sensitive to the temperature structure. The vibrational-rotational lines are therefore probes of the light-absorbing properties of the inner regions.

The estimated fluxes given by the model are sensitive to many of the input parameters. We have run our model by fixing as many parameters as possible from the literature. Our variable parameters are the temperature (T_0) at a distance from the star of 10^{15} cm, the mass-loss rate (\dot{M}), the terminal expansion velocity (v_e) and turbulent velocity (v_t), as well as the inner radius of the CSE (r_i).

Initially we apply a simple, ‘standard model’ of a spherically symmetric and smooth CSE expanding at a constant velocity. Our observational constraints on the structure of the outer part of the wind are given mainly by the radio data, and to a lesser extent, the far-IR ISO data in the same manner as by Ryde et al. (1999c). We later confront this model with the new observational constraints consisting of the absolute fluxes, the radial dependence of the scattered intensity as a function of angular distance, and the two line ratios obtained from photospheric light scattered in vibrational-rotational lines of circumstellar CO.

5.1. The ‘standard’ model

Previous radiative transfer models analysing the CSEs around bright M stars (e.g., Kahane and Jura, 1994) assume large velocity gradients (LVG). The model presented here is a more general code, based on the MC method, with a detailed radiative transport, including non-local effects, and treating the gas in full non-LTE. In the limit where the radiation field does not have a large influence [see for example the discussion on the ‘dusty’ carbon star IRAS 15194-5115 (Ryde et al. 1999c)], non-

³Note the missing cube in their Eq. 3

local effects are not very important. Kahane and Jura (1994) chose an inner radius of 5×10^{14} cm, i.e., approximately $13 R_*$, which is relatively far out in the wind. In our standard model we adopt this value. Note that the dust is supposed to be situated well within this distance.

The turbulent velocity and the expansion velocity of the gas in the CSE are free parameters in the model which we tune together with the other free parameters in order to explain the observed asymmetric radio-line profiles by self-absorption in an optically thick wind, i.e., the mass-loss rate has to be sufficiently large. The temperature at 10^{15} cm (see Eq. 2) we set to $T_0 = 150$ K [a value consistent with those derived from a large survey of optically bright carbon stars (Schöier & Olofsson 2000) where the kinetic temperature structure is obtained in a self-consistent manner]. The mass-loss rate is found to be $2.5 \times 10^{-7} M_\odot \text{ yr}^{-1}$, the terminal expansion velocity is 2.5 km s^{-1} , and the turbulent velocity required is 1.5 km s^{-1} , see Table 1.

In Figure 2 and 3 the model results are shown and compared with some of the observations. We find that it is possible with this model to meet the observational constraints provided by the radio and ISO data reasonably well. The three radio lines are reasonably well reproduced by the model (Figure 2a-c), suggesting a certain importance of self-absorption in the CSE around Mira. Also the modelled fluxes of the lines observed by ISO are reasonably well reproduced (Figure 2d). The scattered, NIR fluxes, as a function of the distance from the star, are shown in Figure 3a and they decline roughly as a power law, with a slope of -3.4 for the R(2) transition. Figure 3b shows the assumed kinetic-temperature law, as well as the excitation temperature for some selected lines, throughout the envelope. The excitation temperatures of the radio lines show that the populations of the lower lying levels of the scattered infrared lines R(1), R(2), and R(3) are not in local thermodynamic equilibrium (LTE).

In Figure 3c the tangential optical depth is shown and gives an indication of the depths-of-formation of the different lines. Furthermore, in Fig. 3d the relative population of level i for the different rotational levels of the two lowest vibrational states of CO for our model are shown as a function of the distance from the star. The popu-

lations of the rotational states of the first excited vibrational state are several orders of magnitude lower than those of the ground level. Furthermore, it can be seen in the figure that these populations vary significantly with the distance from the star, a fact that can not be taken into account in the analytic approach of Ryde et al. (2000).

The angular behaviour of the vibrational-rotational line-intensities and the line ratio of the two R-branch transitions are reasonably well reproduced (Table 2). However, the intensities come out significantly too weak, approximately a factor of 5–10 lower than observed. The maximum optical depth in the line-of-sight is approximately 25, while the radial optical depth is approximately a factor of two higher. We find that by varying the mass-loss rate, the temperature structure and the turbulent velocity, it is not possible to model consistently all the observations.

By introducing a velocity law, i.e., an accelerating wind, it is possible to increase the NIR fluxes derived from the model. Assuming a linearly increasing, with radius, expansion velocity of the CSE, NIR fluxes that are about 2 times larger than in the standard model is possible to obtain.

5.2. The ‘cavity’ model

We find that it is impossible to reach the high fluxes measured in the NIR lines far out in the CSE with a standard wind model extending all the way to the vicinity of the star. There are numerous ways of explaining an observed NIR flux that is lower than expected, but for a higher flux there are not many alternatives. The key problem is to prevent the innermost region of a smooth envelope to lose the radiation by scattering events in a geometrically diverging velocity field. In order to increase the NIR fluxes one can introduce an inner, empty region - i.e., postulate a large inner radius, which will increase the NIR flux at the point where the observations are made.

By moving the inner radius of the CSE further out, high-density material close to the star is removed allowing the central radiation-field to penetrate further out into the wind. This will increase the excitation of the CO molecule, including the low-energy rotational transitions. With a cavity it is possible to explain reasonably well

the FIR fluxes as well as the observations of the NIR vibrational-rotational lines of CO, cf. Tables 2 and 3. However, the radio-line intensities will come out to strong in the model, due to the efficient radiative excitation, and the self-absorption present in these lines will become less pronounced since the optical depth decreases (by approximately a factor of 5 in the radial direction).

We find that an inner boundary at 2.5×10^{15} cm (approximately $1''$ or 53 stellar radii) combined with a mass-loss rate of $\dot{M} = 2.5 \times 10^{-7} M_{\odot} \text{ yr}^{-1}$, i.e., the same as in ‘the standard model’, will result in a sufficiently high flux of stellar radiation reaching the wind regions beyond $2''$ and at the same time enough scatterers at the location of our observations, i.e., at angular distances of $2''$ – $7''$ away from the star. The ISO lines are formed further in than the NIR vibrational-rotational lines, and will start to become sensitive to the adopted inner radius. In the modelling, we have chosen the same temperature structure, velocity structure and turbulent velocity as was obtained from ‘the standard model’.

The results of our best ‘cavity model’ of the CSE around Mira are presented in Tables 2 and 3, where the modelled intensities, line intensity ratios, intensity slopes, the modelled radio-fluxes, and the modelled mean ISO-flux are compared with the observations.

The modelled intensities of the three NIR lines [R(1), R(2), and R(3)] all decline in a $\log I - \log \beta$ -plot with a slope of approximately -3 , which is in good agreement with the observations. Note that there are systematic uncertainties in the R(1) line due to the detector, which will lead to an uncertain R(1)/R(3) ratio [see the discussion by Ryde et al. (2000); this has to be borne in mind when discussing the line ratios].

6. DISCUSSION

The Kitt Peak observations provide our modelling with new, strong constraints. These are the NIR absolute fluxes of the three lowest vibrational-rotational transitions in the R-branch of CO, their radial distributions, and the two line ratios from the three vibrational-rotational lines observed.

We find that it is not possible to meet these new constraints with a ‘standard model’ of the wind, calculated on the basis of the several far-IR ro-

tational transitions within the ground vibrational level of CO as observed by ISO, and radio observations of millimeter rotational transitions of CO; our modelled NIR fluxes are an order of magnitude too low.

By introducing a cavity in order to simulate a higher flux at the point of scattering and keeping the mass-loss rate relatively high, however, we are able to model the NIR fluxes and the brightness distribution, i.e., the decline in the intensity as a function of the distance from the star, providing a slope ($d \log I / d \log \beta$) of approximately -3 . This results in few scatterers on the way and hence increase the number of photons that will be able to be scattered, and, on the other hand, maintains enough scatterers at the point of our observations for the modelled fluxes to be large enough. The important free parameters that couple to each other to give the number density of scatterers are the inner radius (r_i), the mass-loss rate (\dot{M}), and the expansion velocity (v_e).

Thus, in order to reproduce the observed, high NIR fluxes, the radial optical depth should not be too large. If there are too many scatterers on the way radially, many photons will scatter ‘side-ways’ due to the shifts out of the absorption profile caused by the velocity of the flow at a point close to the star and will never make it out to our point of observation. The high optical depths trap the photons as was suggested already by Dyck et al. (1983). Thus, the velocity field is of great importance. If the *geometrical* velocity gradients are large across one optical depth unit (the mean distance between scattering events), the absorption profiles of the absorbing molecules will be shifted with respect to the emission profile of emitting molecules, leading to a decrease in the optical length for the emitted photons. This will lead to a loss of photons and a steepening of the decline of the intensity with distance from the star.

An important quantity for the flux levels at a certain point in the wind is the relation between the expansion velocity, and the turbulent velocity (providing most of the width of the inherent line profiles). If the turbulent velocity, which is of the order of 1 km s^{-1} , is comparable to the wind velocity, the velocity fields will be very important. Also in the case of Mira, this makes the modelling of the CSE sensitive to the ratio between the turbulent velocity and the flow velocity. This is also what

we find; a sensitive parameter in the modelling is this ratio.

A physical reason for a higher flux could be a void of CO molecules, for instance due to an excess UV flux from the white-dwarf companion-star that certainly will partly dissociate CO, or a cavity caused by a decline of the stellar wind to a lower expansion velocity and a lower mass-loss rate, resembling the double wind scenario of Knapp et al. (1998). Other reasons could be that the gas close to the star is in such a state that light is able to pass through relatively unaffected, either due to the medium being clumpy with a low filling factor, or by the matter being in radial structures in the innermost part of the CSE, which, further-out, develops into more smooth or shell-like structures. These structures could occur depending on the expulsion mechanism of matter, such as a non-homogeneous mass-loss due to large convective eddies or magnetic spots, see for example Soker and Clayton (1999). Further reasons could be CO molecules absorbed onto dust grains, which are evaporated further out, or a small radial velocity gradient (i.e., the velocity slowly approaches the terminal velocity of the wind).

For large radial optical depths, the slope ($d\log I/d\log \beta$) will not be constant with distance as is suggested by the observations. In models for which the optical depths are taken to be very large, we find that the slope of the R(3) line is the largest. As a consequence, the line ratios will vary greatly as a function of distance from Mira which again is not observed. The line ratios R(1)/R(3) and R(2)/R(3) increase the further away from the star they are measured. (In a less optically thick model, the slopes will not differ greatly between the three lines and thus neither will the line ratios.) In our observations, however, we will not be able to trace such a trend, having in mind the constraints due to signal-to-noise ratio and the uncertainties involved.

The mass-loss rate determined here, $2.5 \times 10^{-7} M_{\odot} \text{yr}^{-1}$, is in good agreement with the mass-loss rate we estimated using an analytic approach to Mira's wind (Ryde et al. 2000). Note, however, that in this approach the level densities of CO are not known and a mean is estimated, which will lead to an uncertainty, cf. Fig. 3. Also, an assumption in the derivation of the analytical expression for the mass-loss rate is a *tangentially* optically thin

wind, which is not strictly the case for a spherically symmetric and homogeneous wind. In a *tangentially* optically thin wind we expect a decline of the intensity with angular distance, given by a power law with an exponent of -3 . However, even in a *tangentially* optically thick wind we are able to obtain the same $d\log I/d\log \beta = -3$ slope.

The asymmetries in the radio lines, which are optically thick, are caused, in our 'standard model', by self absorption along the line-of-sight. Thus, we are able to reproduce the intensities and radio-line profiles reasonably well without invoking a double-wind scenario as has previously been done in the literature (cf. e.g., Knapp et al., 1998).

7. CONCLUSIONS

In order to reproduce the intensity levels and the angular dependence of the intensity of the vibrational-rotational lines of the CO fundamental band at $4.6 \mu\text{m}$ ($v=1 \rightarrow 0$), it is necessary to require low radial optical-depths to the point of scattering. In a standard CSE model, i.e., a smooth and spherically symmetric wind with an inner radius located fairly close to the central star, the radial optical depths are very large. The photons are scattered already close to the star and, due to the velocity field, shifted out of the absorption profile, leading to an escape. The CSE model that is able to meet these new observational constraints reasonably well needs a form of inner cavity, devoid of gaseous CO. The stellar light is then able to reach further out before it is scattered; the optical depths are reduced significantly. The two CSE models presented here both require a mass-loss rate of $2.5 \times 10^{-7} M_{\odot} \text{yr}^{-1}$ and a turbulent velocity of 1.5 km s^{-1} given an expansion velocity of the wind of 2.5 km s^{-1} . The only parameter that is changed between the two models is the location of the inner radius. In the standard model, that best reproduces the observed radio and FIR emission, we use an inner radius located at approximately $13 R_{*}$ while for the the cavity model, adopted to meet the NIR observational constraints, its location is approximately $50 R_{*}$.

We find that the ratio between the turbulent velocity and the expansion velocity, is of great importance. The flux at $2''$ is sensitive to this ratio; the lower the ratio the lower the observed flux since more photons are lost 'sideways' due to ve-

locity shifts out of the absorption profile. Furthermore, we conclude that for modelling vibrational-rotational lines the approximation of CRD is not a bad assumption as long as the optical depths are not too large.

The NIR observations in combination with a model of the CSE is providing us with new pieces of information on the inner-most regions of the wind. The properties of this inner wind, that is simulated in the model by a void of CO, can be explained physically by structures of the gas close to the star (within approximately $2''$) that are in such a form that light is able to pass through. Further observations of the gas in the stellar wind of Mira slightly closer to the star could therefore be rewarding.

The inner parts of the circumstellar environment are complicated regions of which we have a very limited understanding (see e.g., Ryde et al., 1999a), and where many of the basic assumptions of our model are certainly not valid. Thus, the model could fail in describing reality. We need further observational constraints. The Phoenix spectrometer makes it possible to use long-slit spectroscopy, which makes spatially resolved spectra along the slit attainable. The slit is then used to map the CSE. However, no interferometric mappings of the CSE of Mira with a high enough spatial resolution exist. Planesas et al. (1990b) presented observations with a resolution of $7.8'' \times 5.4''$ using the Owens Valley millimeter-wave interferometer. The IRAM interferometer at Plateau de Bure can provide a spatial resolution of under $1''$.

We are very grateful for inspiration from, and enlightening discussions with B. Gustafsson, H. Olofsson, and K. Eriksson. The referee is thanked for valuable suggestions. This research was supported by the Swedish National Space Board, the Swedish Natural Science Research Council, and the Royal Swedish Academy of Sciences.

REFERENCES

- Bernes, C., 1979, *A&A* 73, 67
- Bester, M., Danchi, W. C., Degiacomi, C. G., Townes, C. H., and Geballe, T. R., 1991, *ApJ* 367, L27
- Clegg, P., Ade, P., Armand, C., et al., 1996, *A&A* 315, L38
- Crosas, M. and Menten, K. M., 1997, *ApJ* 483, 913
- Crosas, M., Menten, K. M., Young, K., and Phillips, T. G., 1997, *Ap&SS* 251, 189
- Danchi, W. C., Bester, M., Degiacomi, C. G., Greenhill, L. J., and Townes, C. H., 1994, *AJ* 107, 1469
- Dyck, H. M., Beckwith, S., and Zuckerman, B., 1983 *ApJ* 271, L79
- ESA, 1997, ESA, The Hipparcos and Tycho Catalogues, ESA SP-1200
- Glassgold, A. E., 1996, *ARA&A* 34, 241
- Goldreich, P. and Scoville, N., 1976, *ApJ* 205, 144
- Groenewegen, M. A. T., 1994, *A&A* 290, 531
- Gustafsson, B. and Ryde, N., 2000, in: B. Wing (ed.) *Proc. IAU Symp. 177, The Carbon Star Phenomenon*. Kluwer, Dordrecht, p. 481
- Haniff, C. A., Ghez, A. M., Gorham, P. W., et al., 1992, *AJ* 103, 1662
- Haniff, C. A., Scholz, M., and Tuthill, P. G., 1995, *MNRAS* 276, 640
- Huré, J. M. and Roueff, E., 1996, *A&AS* 117, 561
- Kahane, C. and Jura, M., 1994, *A&A* 290, 183
- Karovska, M., Hack, W., Raymond, J., and Guinan, E., 1997, *ApJ* 482, L175
- Karovska, M., Nisenson, P., and Beletic, J., 1993, *ApJ* 402, 311
- Karovska, M., Nisenson, P., Papaliolios, C., and Boyle, R. P., 1991, *ApJ* 374, L51
- Kessler, M. F., Steinz, J. A., Anderegg, M. E., et al., 1996, *A&A* 315, L27
- Kirby-Docken, K. and Liu, B., 1978, *ApJS* 36, 359
- Knapp, G. R., Young, K., Lee, E., and Jorissen, A., 1998, *ApJS* 117, 209
- Kwan, J. and Webster, Z., 1993, *ApJ* 419, 674

- Lopez, B., Danchi, W. C., Bester, M., et al., 1997, ApJ 488, 807
- Mahler, T. A., Wasatonic, R., and Guinan, E. F., 1997, Informational Bulletin on Variable Stars 4500, 1
- Mamon, G. A., Glassgold, A. E., and Huggins, P. J., 1988, ApJ 328, 797
- Netzer, N. and Knapp, G. R., 1987, ApJ 323, 734
- Neufeld, D. A. and Kaufman, M. J., 1993, ApJ 418, 263
- Olofsson, H., 1996, Ap&SS 245, 169
- Olofsson, H., Bergman, P., Eriksson, K., and Gustafsson, B., 1996, A&A 311, 587
- Planesas, P., Bachiller, R., Martin-Pintado, J., and Bujarrabal, V., 1990a, ApJ 351, 263
- Planesas, P., Kenney, J. D. P., and Bachiller, R., 1990b, ApJ 364, L9
- Quirrenbach, A., Mozurkewich, D., Armstrong, J. T., et al., 1992, A&A 259, L19
- Ryde, N., Eriksson, K., and Gustafsson, B., 1999a, A&A 341, 579
- Ryde, N., Gustafsson, B., Eriksson, K., and Hinkle, K. H., 2000, ApJ in press
- Ryde, N., Gustafsson, B., Hinkle, K. H., Eriksson, K., Lambert, D. L., and Olofsson, H., 1999b, A&A 347, L35
- Ryde, N., Schöier, F. L., and Olofsson, H., 1999c, A&A 345, 841
- Schöier, F. L., 2000, PhD thesis, Stockholm Observatory
- Schöier, F. L., and Olofsson, H., 2000, A&A submitted
- Soker, N. and Clayton, G. C., 1999, MNRAS 307, 993
- Stickland, D. J., Cassatella, D., and Ponz, D., 1982, MNRAS 199, 1113
- Stanek, K. Z., Knapp, G. R., Young, K., and Phillips, T. G., 1995, ApJS 100, 169
- Stickland et al. (1982)
- Swinyard, B., Clegg, P., Ade, P., et al., 1996, A&A 315, L43
- Van Leeuwen, F., Feast, M. W., Whitelock, P. A., and Yudin, B., 1997, MNRAS 287, 955
- Wilson, R. W., Baldwin, J. E., Buscher, D. F., and Warner, P. J., 1992, MNRAS 257, 369
- Young, K., 1995, ApJ 445, 872

Fig. 1.— The *o* Ceti light-curve. 1998 October 29 corresponds to a Julian date of 2451116. At that time *o* Ceti had a visual magnitude of 7.8 and was in a pre-maximum phase. (Mattei, J. A., 1999, Observations from the AAVSO International Database, private communication).

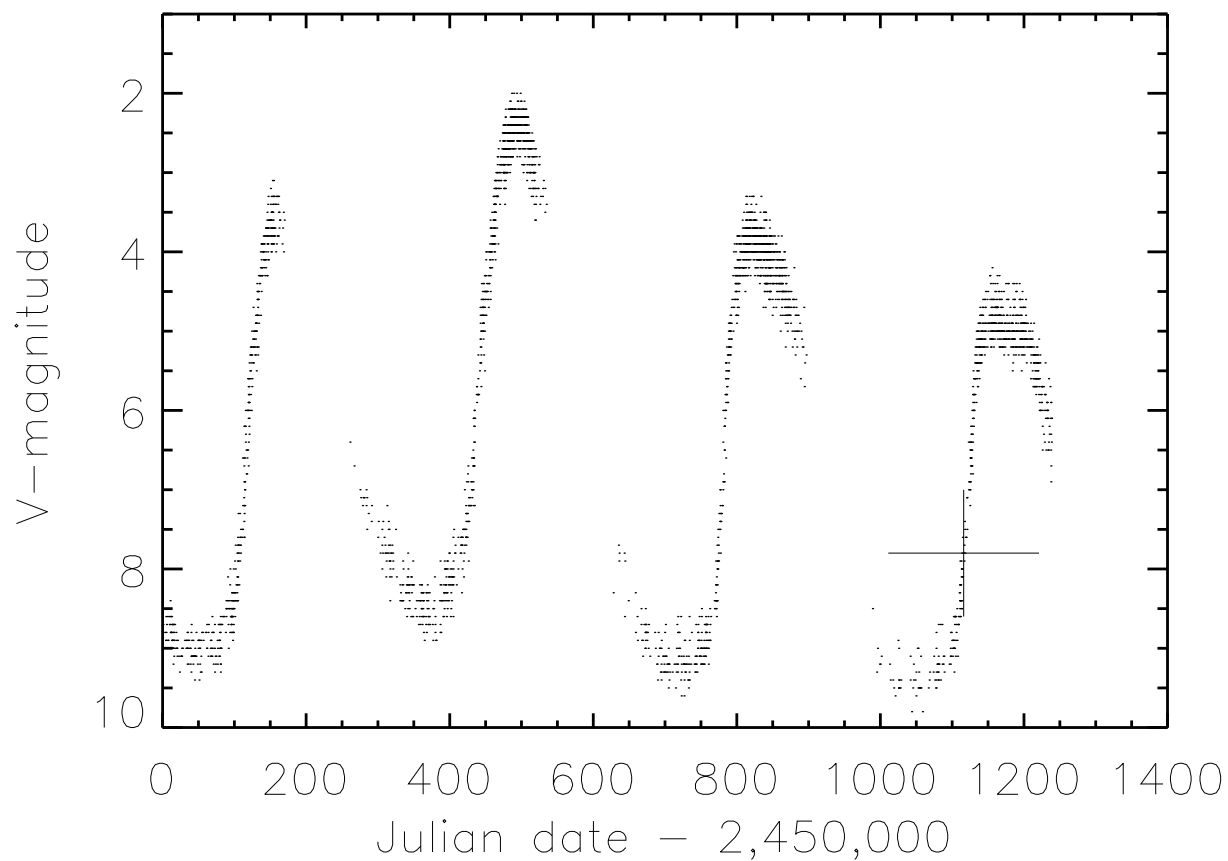


Fig. 2.— Modelling results for the best standard model of Mira’s wind. a-c) The JCMT millimeter-wave observations, in main-beam brightness temperature, overlaid with the model line-profiles. The beam size used is indicated in the upper right-hand corner of each panel. Note that for the CO($J=3\rightarrow 2$) we also show a scaled line profile for easier comparison with the observed shape of the emission line. d) ISO observations and the model overlays using a beam size of 70".

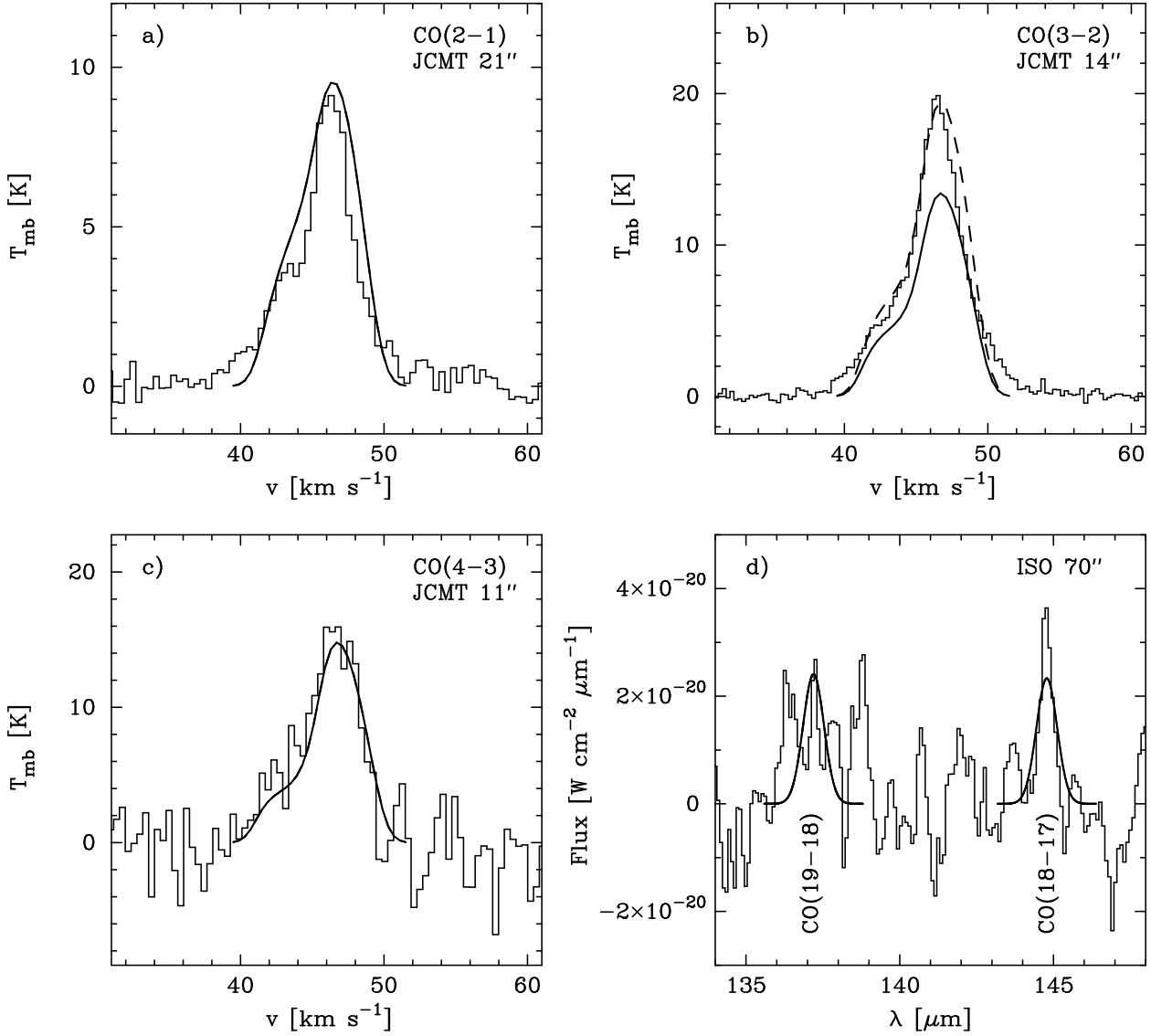


Fig. 3.— Modelling results for the best standard model of Mira’s wind. a) The intensity of the NIR emission lines R(1) (full), R(2) (dashed), and R(3) (dash-dotted) as a function of the distance (in cm and arcseconds) from the star. b) The kinetic temperature structure of the model of the circumstellar envelope, given by a power law, is shown as a thick full line. The three other lines show the calculated excitation-temperature structure of the infrared R(2)-line (dotted), the radio CO($J=3\rightarrow 2$) line (dashed), and the far-infrared CO($J=18\rightarrow 17$) line (dash-dotted). All lines are non-thermal. The CO($J=18\rightarrow 17$) line is shown only out to $r=1\times 10^{16}$ cm since beyond this radius these levels are scarcely populated, see Fig. 3^d. c) The tangential optical depths of three selected lines (symbols same as in b). These give an indication of how far out in the wind the lines are formed. d) Relative level-populations according to our best model of Mira’s wind. In the model we include 30 rotational levels each in the two lowest-lying vibrational states. For clarity, only 10 rotational levels from each of the two vibrational levels are shown. The upper set of graphs represent the populations of the rotational levels in the ground vibrational state ($v=0$), i.e., $J=0-10$. The lower set of graphs represent the excited vibrational state $v=1$. For instance, the R(1) line is a transition from ($v=1$, $J=2$) to ($v=0$, $J=1$).

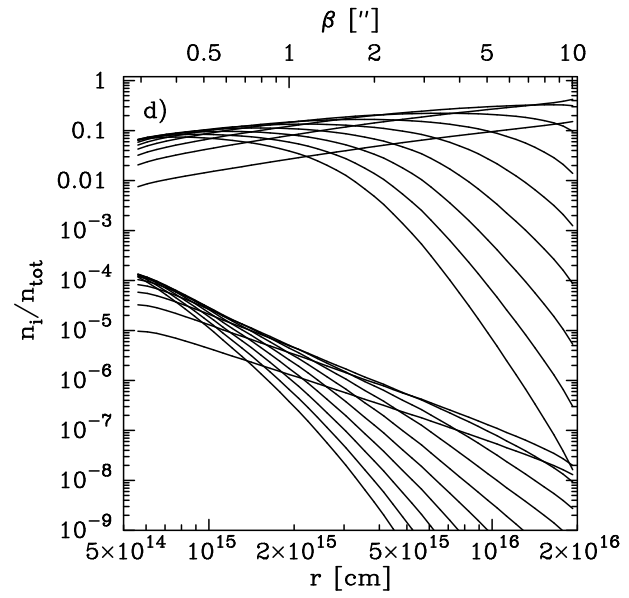
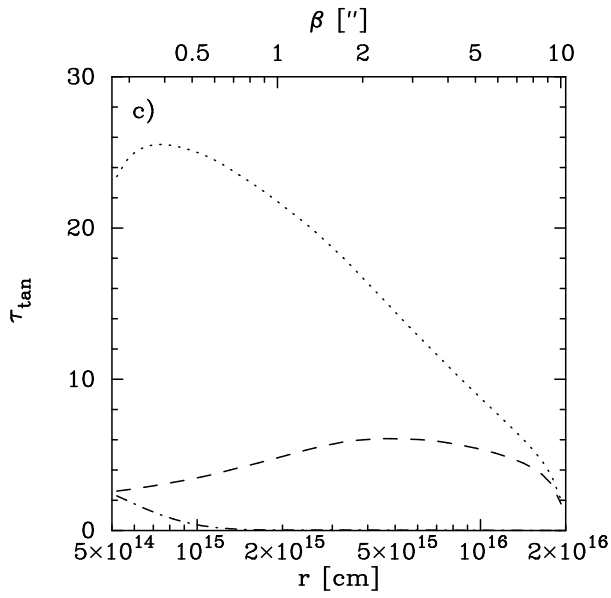
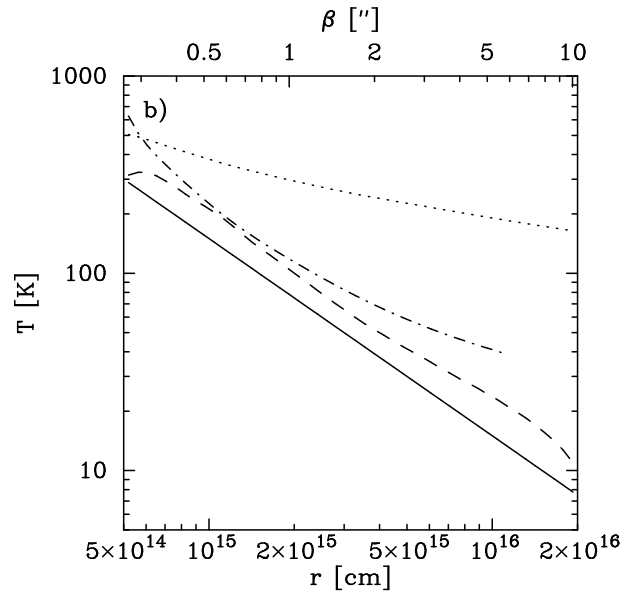
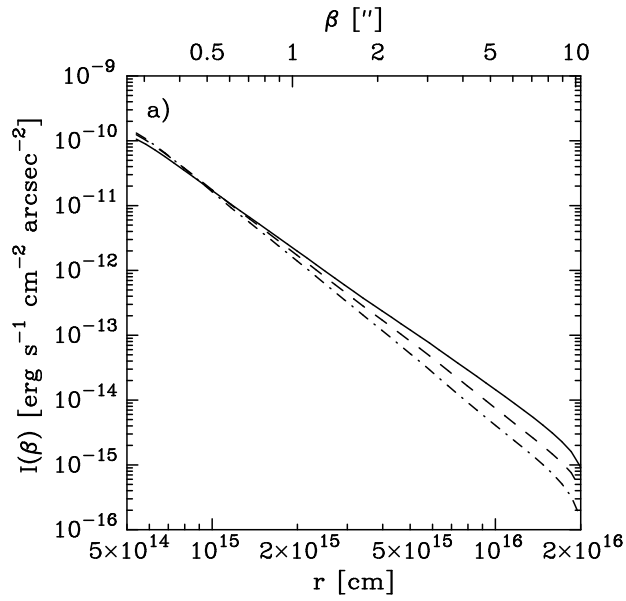


TABLE 1
 THE PARAMETERS ADOPTED FOR THE CSE AROUND α CETI

Model parameter	Value
T_*	2400 K
T_d	1100 K
L_{bol}	8900 L_\odot
L_*	7100 L_\odot
L_d	1800 L_\odot
R_*	3.8×10^{13} cm
R_d	3 R_*
D	128 pc
\dot{M}	$2.5 \times 10^{-7} M_\odot \text{ yr}^{-1}$
f_{CO}	5×10^{-4}
v_e	2.5 km s^{-1}
r_p	2.0×10^{16} cm
$r_{\text{i,standard}}$	5.0×10^{14} cm
$r_{\text{i,cavity}}$	2.5×10^{15} cm
v_t	1.5 km s^{-1}
T_0	150 K
R_0	1.0×10^{15} cm

TABLE 2

INTENSITIES IN $10^{-12} \text{ ERG S}^{-1} \text{ CM}^{-2} \text{ ARCSEC}^{-2}$ (MEASURED AT $2''$), THE LINE INTENSITY RATIOS (AVERAGED OVER $2 - 3.4''$), AND THE VARIATION OF THE R(2) INTENSITY WITH DISTANCE FROM THE STAR.

	$I[\text{R}(1)]$	$I[\text{R}(2)]$	$I[\text{R}(3)]$	$\frac{\text{R}(1)}{\text{R}(3)}$	$\frac{\text{R}(2)}{\text{R}(3)}$	$\frac{d \log I[\text{R}(2)]}{d \log \beta}$
Observed:	2.1 ± 1.0	1.5 ± 0.8	1.2 ± 0.6	1.7 ± 0.6	1.2 ± 0.2	-2.8 ± 0.4
Modelled ('standard'):	0.24	0.16	0.11	2.2	1.5	-3.4
Modelled ('cavity'):	1.21	1.18	1.12	1.3	1.1	-3.0

TABLE 3

THE INTEGRATED RADIO FLUX IN K km s^{-1} , AND THE AVERAGED ISO FLUX IN $10^{-20} \text{ W cm}^{-2}$.

	CO($J=2 \rightarrow 1$)	CO($J=3 \rightarrow 2$)	CO($J=4 \rightarrow 3$)	ISO flux
Observed:	44 ± 9	94 ± 19	77 ± 15	2 ± 1
Modelled ('standard'):	50	67	71	2.0
Modelled ('cavity'):	72	147	178	2.1